

Effect of organic corrosion inhibitors functional groups (azo and azomethine) on carbon steel N80 alloy corrosion using the electrochemical polarization technique

A.M. Jabbar^{ID}* and A.S. Abdulnabi^{ID}**

Chemistry Department, Education College for Pure Sciences, Basrah University, Basrah
61001, Iraq

E-mail: *abeer.mohammed@buog.edu.iq; **adnan.abdulnabi@uobasrah.edu.iq

Abstract

This study prepared the azo compound (A) and the Schiff base compound (S) from the same amine compound 3-aminopyridine. The identity of these two prepared compounds was confirmed using several techniques: via FT-IR, UV-vis, ¹H NMR, ¹³C NMR, EI-Mass, SEM, and EDS spectroscopic techniques. These two compounds were applied as corrosion inhibitors for carbon steel N80 by taking several molar concentrations: 0.0001; 0.0005; 0.001 and 0.005 M, at different temperatures of 298, 308 and 318 K in an acidic medium of HCl at a concentration of one molar. The technique used in this study is electrochemical polarization (Tafel curves). The results obtained from this study confirmed that the corrosion current is high in the absence of inhibitors but decreases in the presence of inhibitors. Also, the corrosion current is inversely proportional to the increase in concentrations of organic inhibitors and directly proportional to the temperature increase. Besides, the percentage of inhibition efficiency increases with increasing temperature, indicating that the adsorption is chemisorption. We also studied the activation energy, and the following thermodynamic parameters have been calculated from the Langmuir adsorption isotherm: free energy (ΔG^0), enthalpy (ΔH^0) and entropy change (ΔS^0). This electrochemical method (Tafel extrapolation) and SEM and EDS techniques have confirmed that these prepared inhibitors are effective against corrosion through the formation of a protective film on the surface of carbon steel.

Received: November 25, 2023 Published: January 22, 2024

doi: [10.17675/2305-6894-2024-13-1-9](https://doi.org/10.17675/2305-6894-2024-13-1-9)

Keywords: *electrochemical polarization, organic inhibitors, activation energy, corrosion potentials, corrosion rates.*

1. Introduction

Corrosion is a process that may be natural, chemical, or electrochemical and is also considered a universal phenomenon of metals returning to their natural form in the environment [1]. However, the world economy will suffer an enormous loss due to corrosion [2]. The pure forms of most alloys and metals are highly reactive and easily decompose due to corrosion due to their interaction with the components of the environment [3]. There are diverse ways to lessen or prohibit corrosion, including organic corrosion inhibitors [4]. It is

widely utilized in numerous industries and is regarded as one method of protecting metal surfaces from corrosion due to their effectiveness at a vast range of temperatures, compatibility with protected materials, suitable solubility in water, low cost and relatively inferior toxicity. Organic corrosion inhibitors adsorb on the surface to create a protective layer that replaces water and protects it against damage [5]. The presence of polar functional groups with S, O or N atoms in the molecule, heterocyclic compounds, and pi electrons also increases the efficiency of these organic corrosion inhibitors. The adsorption of the molecule on the metal surface depends on the polar function of the molecule. The organic compound containing oxygen, nitrogen and/or sulfur blocked the active corrosion sites by adsorbing the metallic surface and the metal surface was adsorbed with an organic corrosion compound to form a protective film that displaces water from the metal surface and protects it against corrosion [6]. The presence of the P atom in an organic compound inhibitor was more than active to close active sites from S, N and O in different structures; therefore, that coincides with these atoms with the performance of the inhibitor and reduces the corrosion attack on the metal [7]. Current studies show that numerous organic inhibitors are adsorbed on the outer surface of the metal surface by expelling water molecules from the outer surface and creating a dense film wall. The possibility of obtaining a lone electron pair and π -electrons in the inhibitor molecules leads to accelerating the process of electron transfer from the inhibitor to the metal, and thus, a coordinate covalent bond is formed responsible for transferring electrons from the inhibitor to the outer surface of the metal [8]. The strength of the bond for chemisorption is affected by the density of electrons of the atom donating the functional group, in addition to the polarizability of the group. The inhibition process increases whenever the hydrogen atom attached to the carbon atom inside the aromatic ring is replaced by a substituent group such as [9] $-\text{NH}_2$, NO_2 , $-\text{CHO}$ or $-\text{CHO}$.

2. Material and Instrument

The substances utilized in this experiment are as follows: 3-aminopyridine, 3,4-ethylenedioxy benzaldehyde, and 4-chloro-3,5-dimethyl phenol are provided by Pallav, Alfa Aesar, and Merck, respectively. The rest of the vehicles used are from Sigma Aldrich Company. The purity of all these compounds was 99%. For the study, we utilized the carbon steel alloy N80, its dimensions are 3, 2 and 0.2 length, width, and thickness respectively, and the weight percent of the components was: 0.3C, 0.006Si, 0.05P, 1.5Mn, and the rest of Fe. The FT-IR spectra were recorded on a Shimadzu FT-IR 8400S spectrometer using a KBr disk in the range $4000\text{--}500\text{ cm}^{-1}$. ^1H NMR spectra were collected using a Bruker 500 spectrometer using tetramethylsilane (TMS) as an internal reference. The chemicals' mass spectra were captured using an Agilent Technologies 5975C mass spectrometer (EI, 70 eV). The UV-visible spectra were collected using a Japan PD303 UV-visible spectrophotometer. Scanning electron microscopy (SEM) was utilized to study the materials' surface morphology. An SEM JEOL JSM-5400 was employed for the experiment. HCl was

employed to make the attacker media. Dilution with distilled water yielded a sufficient concentration of HCl acid.

3. Synthesis of Compounds

3.1. Preparation of an inhibitor of azo compound (A)

Azo ligands were prepared using the traditional method [10, 11]. It is summarized in two steps. The first step, which is the diazotization process, includes mixing 0.006 moles (0.5646 g) from 3-aminopyridine compounds with 2.1 ml of concentrated hydrochloric acid with 12 ml of distilled water, followed by cooling the mixture in an ice bath to a temperature of (0–5°C). 0.006 mole (0.456 g) of sodium nitrite was dissolved in 6 ml of distilled water and placed in an ice bath until the temperature (0–5°C) was reached. The prepared sodium nitrite solution was added drop by drop with continuous stirring using a magnetic stirrer, ensuring the temperature did not rise above (5°C). After that, the solution was left to settle for 30 minutes to complete the diazotization reaction. A change in the color of the solution was observed, indicating the formation of the diazonium salt. 0.006 mole (0.9396 g) of 4-chloro-3,5-dimethylphenol was dissolved in 100 ml of distilled water containing 1.8 g of sodium hydroxide, and the prepared phenol solution was cooled in an ice bath to a temperature of (0–5°C). The second step was the coupling reaction, in which the resulting diazonium salt solution was added drop by drop to the prepared basic phenol solution with continuous stirring for (1–2) hours, and the temperature was maintained at (0–5°C). We notice the formation of a reddish-brown precipitate. The reaction mixture precipitated for 24 hours in a cold place. The acid pH was adjusted to reach 6, and then, the sediment was collected, filtered, washed with distilled water, and dried. It was recrystallized twice in hot ethanol and hexane. The melting point was (161–162°C, 76% yield).

3.2. Preparation of an inhibitor of Schiff base (S)[12]

The Schiff base was prepared by reflux distillation reaction between mixing 0.006 mole (0.9849 g) of 3,4-ethylenedioxy benzaldehyde dissolved in 12 ml ethanol and using a round flask of capacity 100 ml and 0.006 mole (0.5646 g) of 3-aminopyridine dissolved in 12 ml ethanol and the reaction followed by the addition of 3 drops glacial acetic acid. The mixture was refluxed and monitored using TLC (*n*-hexane: ethyl acetate/60:40) for 14 hours. The products forming a greenish-yellow crystalline precipitate were washed and dried to obtain an inhibitor. It was recrystallized using hot tetrahydrofuran (THF) to obtain the product in its pure form (melting point 75–76°C, 70% yield).

3.3 Preparing concentrations of compounds A and S

A series of concentrations from dilution HCl 1 M were prepared to study electrochemical polarization (Tafel curve) on carbon steel N80. This specimen of carbon steel 3, 2 and 0.2

centimeter in terms of length, width, and thickness, respectively, has been immersed in 0.0001, 0.0005, 0.001 and 0.005 M of inhibitors **A** and **S**.

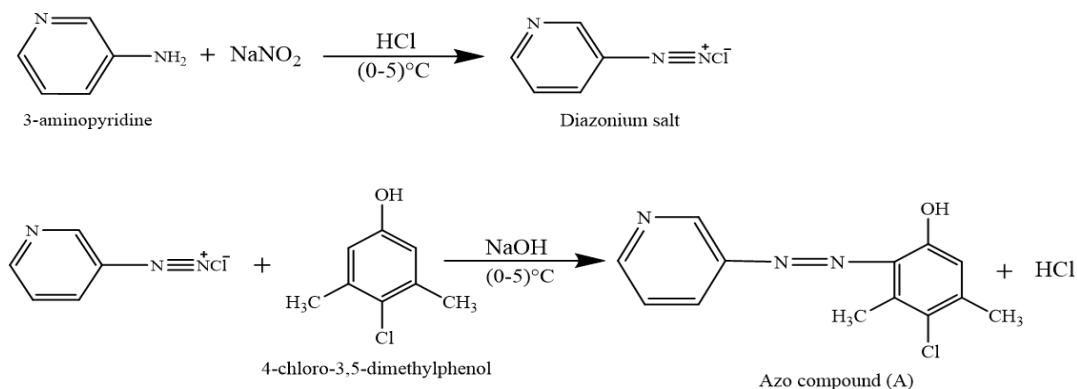


Figure 1. Preparation of azo compound (**A**).

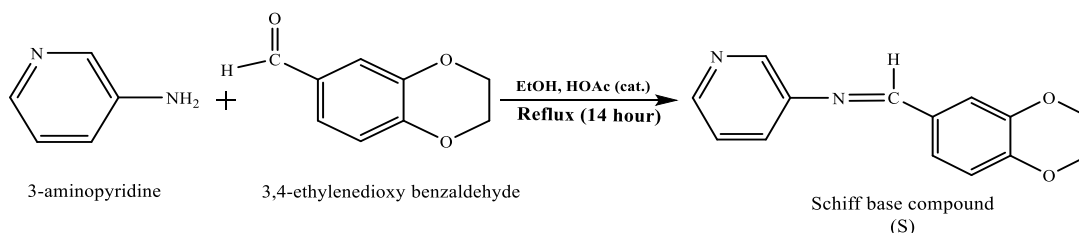


Figure 2. Preparation of Schiff base (**S**).

4. Results and Discussion

4.1. Chemistry

Many techniques have verified the compound's (**A** and **S**) identity. FT-IR, UV-Vis, ¹H NMR, ¹³C NMR and EI-Mass. Which displays the FT-IR (KBr, cm⁻¹) spectrum [13] of (**A**) compound: a stretching vibration band of the (OH) group appears, which is broad at the range (3388.93–3441.01), N=N group appears at 1438.90, C=N ring appears at 1583.5. Also, **S** compound: C=N azomethine group appears at 1660.71, C=N ring appears at 1600.92. As well as both compounds containing the bands in the range 3003.17–3072.62 return to the C–H aromatic group, and 2818–2968.45 return to the C–H aliphatic group, and C=C at 1431.18–1612. The *U_v*–*V_{is}* (nm) spectrum [14] exhibits electronic transitions for π–π* (N=N) appearing at 360, *n*–π* (C=N) azomethine appearing at 353 and both compounds show π–π* at 259.5 and 243.5 for aromatic rings **A** and **S** respectively. The chemical shift of ¹H NMR spectrum (500 MHz, DMSO-d₆) for the **A** compound is 9.85 ppm (s, 1H, OH), 6.49–9.29 ppm (m, 5H, Ar-H), 2.132.25 ppm (s, 6H, CH₃). And **S** compound: 9.67 ppm (s, 1H, N=CH), 6.68–8.56 ppm (m, 7H, phenyl ring) and 3.03 ppm (d, 4H, –O–CH₂).

Moreover, the chemical shift for ¹³C NMR spectrum [15] 125 MHz, DMSO-d₆ demonstrate for **A** compound: 30.88 ppm (methyl carbon), 115.98–157.31 ppm (aromatic

carbon), and 143.31 ppm ($-\text{C}=\text{N}$ ring). The *S* compound illustrates: 21.62 ppm methyl carbon, 111.53–154.66 ppm aromatic carbon, 162.39 ppm ($-\text{C}=\text{N}$ Schiff) and 143.50 ppm ($-\text{C}=\text{N}$ ring). EI-Mass spectroscopy [16] m/z (%) for **A** compound: 261.1 (M^+ , 58.1) and **S** compound: 239.2 (M^+ , 225.2).

4.2. Electrochemical experiments

4.2.1. Polarization curves [17]

Polarization curves were studied in acidic media with a 1 M concentration of hydrochloric acid solution immersed in carbon steel N80 alloy in the presence and absence of different concentrations of inhibitors and at different absolute temperatures. This measurement was within the range of ± 400 mV. We notice from Figures 3 and 4 for compounds *A* and *S* at 318 K that with an increase in the concentration of these two inhibitors, a slight deviation occurs in the values of corrosion potentials (E_{corr}), starting from the negative region, which is the region of iron ions being released from the surface of carbon steel N80 to the more positive values, which indicate the formation of a protective film on the surface of the metal, causing a decrease in the values of corrosion current. If the corrosion potential (E_{corr}) exceeds 80 mV, the inhibitor is cathodic or anodic. Meanwhile, the corrosion potential (E_{corr}) is 50 mV which means both inhibitors are mixed-type. And this indicates that when both inhibitors are added to the acidic media, it will impede the anodic reactions and delay the process of hydrogen gas release during the cathodic reaction [18].

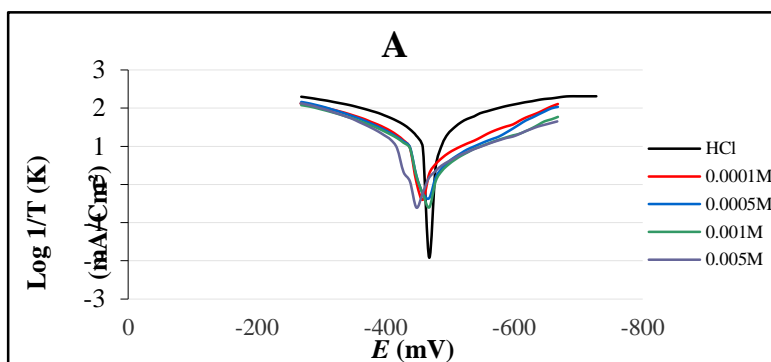


Figure 3. Polarization curve (Tafel plot) of compound **A**.

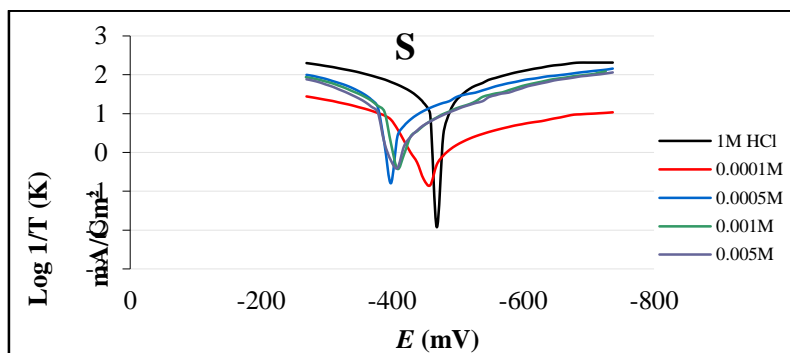
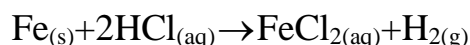


Figure 4. Polarization curve (Tafel plot) of compound **S**.

In Table 1, the data of the anodic (β_a) and cathodic (β_c) Tafel slopes are obtained from the β_a and β_c polarization curves, respectively. We also notice soft changes in the values of the β_a and β_c slopes [19]. When there are different concentrations of inhibitors **A** and **S**, this indicates the adsorption of molecules of the two inhibitors on both the cathodic and anodic sites. General reactions in the HCl medium give the equation:



Dissociation of iron for anodic reaction in the acid:



Cathodic reaction to release hydrogen gas:



From both tables, we notice that the corrosion current density values are high in the absence of inhibitors **A** and **S**. This causes the metal to decompose, releasing iron ions in the anodic reaction, generating electrons that will be consumed in the cathodic reaction, and releasing hydrogen gas, which reduces the pH value, which assists in increasing the corrosion current density (i_{corr}). In the presence of inhibitors, **A** and **S**, the value of i_{corr} will decrease and decrease further with the increase in the concentration of the inhibitors used, and i_{corr} increases with increased temperature, whereas decreasing with an increase in concentration for inhibitors [20].

Table 1. Data on polarization curves for corrosion of carbon steel N80 at various concentrations of **A** and **S** inhibitors at various temperatures.

Comp.	Temp. [K]	Conc. of inh. [M]	$-E_{\text{corr}}$ [mV]	i_{corr} [mA/cm ²]	β_a [mV/Dec]	β_c [mV/Dec]	CR [mpy]	IE%	θ
Blank HCl	298		446	5.03	84.2	-235	2.29	–	–
	308	1	443	14.27	159.3	-148	6.50	–	–
	318		448	31.03	207.7	-210.8	14.13	–	–

Comp.	Temp. [K]	Conc. of inh. [M]	$-E_{\text{corr}}$ [mV]	i_{corr} [mA/cm ²]	β_a [mV/Dec]	β_c [mV/Dec]	CR [mpy]	IE%	θ
A	298	0.0001	469.2	4.52	100.5	-158.5	2.05	10.13	0.1
	308		468.1	5.69	115.2	-154.3	2.59	60.12	0.6
	318		458.1	12.05	145.8	-184.5	5.48	61.16	0.61
	298	0.0005	474.5	3.59	78.1	-143.8	1.63	28.62	0.28
	308		468.4	5.17	94.1	-156.3	2.35	63.77	0.63
	318		461	6.19	97.8	-147.2	2.81	80.05	0.8
	298	0.001	467.2	1.89	72.9	-194.2	0.86	62.42	0.62
	308		468	2.34	101.4	-186	1.06	83.6	0.83
	318		468.6	2.9	85.2	-150.2	1.32	90.65	0.9
	298	0.005	448	1.17	48.3	-173.6	0.53	76.73	0.76
	308		449	1.27	64.3	-154.4	0.57	91.1	0.91
	318		449.5	1.55	50.1	-117.7	0.7	95	0.95
S	298	0.0001	458.6	4.39	108.1	-390	1.99	12.72	0.12
	308		469	5.28	73.9	-113.6	2.40	62.99	0.62
	318		456.2	6.98	307.8	-161.1	3.17	77.5	0.77
	298	0.0005	457.4	2.91	67	-157.2	1.32	42.14	0.42
	308		409.1	3.24	80.3	-399.7	1.47	77.29	0.77
	318		397.7	4.43	56.8	-109.3	2.01	85.72	0.85
	298	0.001	418.9	1.14	41.7	-111.8	0.51	71.96	0.71
	308		408.8	1.64	36.6	-82.5	0.74	88.5	0.88
	318		408.6	1.65	37	-85.4	0.75	94.68	0.94
	298	0.005	417.9	1.02	38.7	-84.1	0.46	79.72	0.79
	308		408	1.04	39	-67.4	0.47	92.71	0.92
	318		408.1	1.44	47.1	-75.8	0.65	95.35	0.95

The Schiff base (S) inhibitor is more effective in the inhibition process than the azo compound (A) in acidic environments, and the reason is due to the effectiveness of the azomethine group.

4.2.2. Study of corrosion rates (CR) and inhibition effectiveness (IE)

From the two tables above, the percentage of inhibition efficiency (%IE) and the degree of surface coverage (θ) of the submerged alloy can be computed using the corrosion current density numbers. Through the Equations below 1 and 2.

$$\%IE = \left[\frac{i_{\text{corr.uninh}} - i_{\text{corr.inh}}}{i_{\text{corr.uninh}}} \right] \cdot 100 \tag{1}$$

$$\theta = \frac{i_{\text{corr.uninh}} - i_{\text{corr.inh}}}{i_{\text{corr.uninh}}} \tag{2}$$

We observe that the %IE or protection of carbon steel and the θ increase with increasing concentrations of organic inhibitors. It is directly proportional to the increase in temps due to the adsorption of organic inhibitor molecules and the strength of their adsorption on the surface of the alloy [21]. Figures 5 and 6 show the correlation between the (IE%) and temperatures for both inhibitors A and S. Moreover, the corrosion rate (CR) values for carbon steel N80 in the absence of inhibitors A and S are relatively high and can be attributed to the decomposition of the metal in the anodic reaction. By adding the two inhibitors with higher concentrations, the rate of corrosion declines and the IE% increases [22].

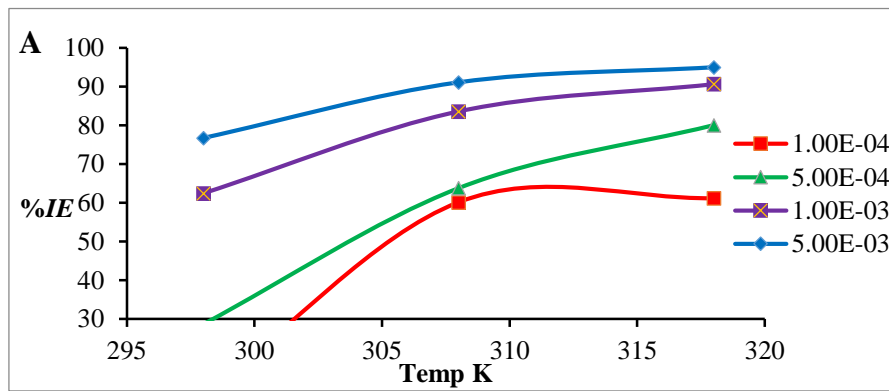


Figure 5. (IE%) vs. temperature at various concentrations of inhibitor (A).

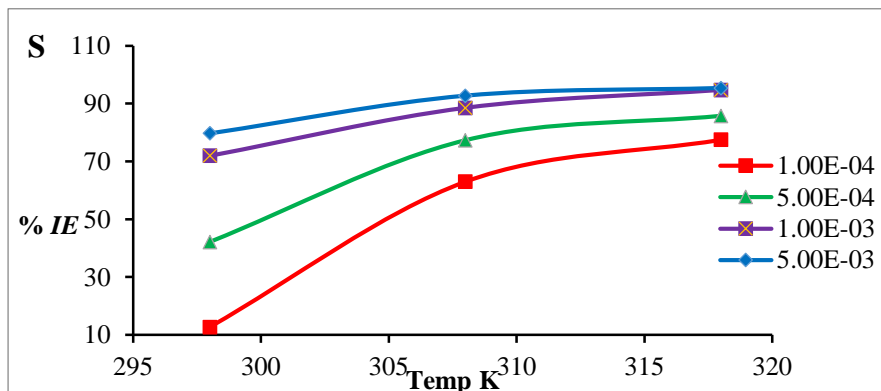
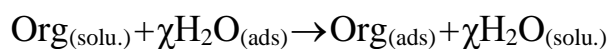


Figure 6. (IE%) vs. temperature at various concentrations of inhibitor (S).

4.2.3. Adsorption isotherm

The method of Tafel extrapolation should be used to calculate data on θ at various inhibitor amounts to comprehend the adsorption and corrosion inhibition mechanisms behavior of the inhibitor molecules upon carbon steel N80 superficies.

The displacement of water molecules adsorbed on the metal surface is the process by which organic molecules of inhibitors are adsorbed, as in Equation 3 below.



The study of adsorption isotherms reveals crucial details about how the inhibitors interact with the metal surface using the Langmuir equation [23].

$$\frac{C}{\theta} = \frac{1}{K_{\text{ads}}} + C \quad (3)$$

The symbols C , θ , and K_{ads} represent the inhibitor's concentration, coverage of the surface, and metal–inhibitor interaction equilibrium constant, respectively. Figures 7, 8 for inhibitors **A** and **S** show a drawing of the Langmuir relationship at different temperatures between C/θ vs C to give a straight line, through which the value of R^2 for the isotherm model presented in Tabel 2 for the data fit into Langmuir, which Langmuir isotherm with R^2 values of approaches 0.99. Indicates the occurrence of interfacial interference in the inhibitor components and indicates the completion of the Langmuir model. Therefore, Langmuir isotherm adsorption is appropriate for evaluating the adsorption equilibrium constant K_{ads} .

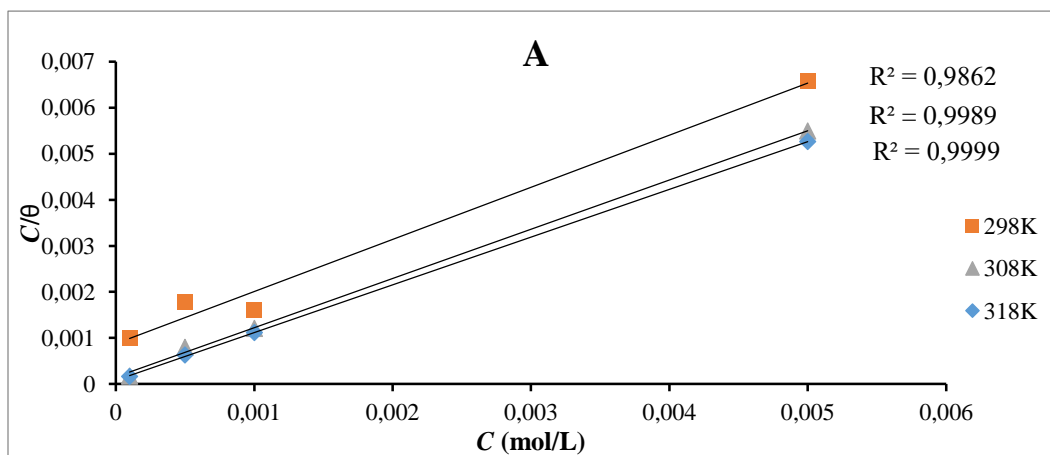


Figure 7. Langmuir adsorption isotherms (A).

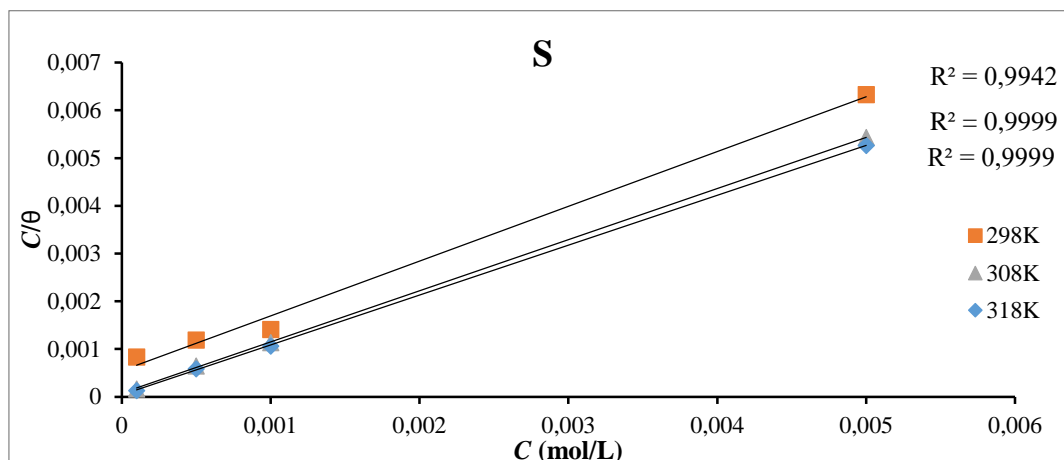


Figure 8. Langmuir adsorption isotherms (**S**).

From the intercept value, the value of K_{ads} is high, indicates that the adsorption process of both inhibitors **A** and **S** on the surface of the carbon steel N80 alloy is too high. The value of K_{ads} leads to calculating [24] the Gibbs free energy (ΔG_{ads}^0) through Equation 4 below.

$$\Delta G_{\text{ads}}^0 = -RT \ln(K_{\text{ads}} \cdot 55.5) \quad (4)$$

R , T and K refer to the universal gas constant, absolute temp, and equilibrium constant, respectively 55.5 denotes the molar concentration of water particles in solution mol/L. From Table 2, we notice that the free energy values are negative, and this signifies that the adsorption process on the metal surface is spontaneous.

Table 2. Parameters of the adsorption Langmuir isotherm of the (**A** and **S**) inhibitory on the carbon steel surface at all studied temperatures (298 to 318 K).

Inhibitor	Temp. [K]	R^2	K_{ads}	$\text{Log}K_{\text{ads}}$	ΔG_{ads}^0 [kJ/mol]	ΔH_{ads}^0 [kJ/mol]	ΔS_{ads}^0 [J/mol·K ⁻¹]
A	298	0.9862	1824.40	3.0566	-27.3882		410.1
	308	0.9989	12946.98	3.8276	-32.8536	94.8465	414.6
	318	0.9999	27062.63	4.0969	-35.5599		410.0
S	298	0.9942	1139.20	3.2611	-28.5549		454.0
	308	0.9999	6724.51	4.1121	-34.5312	106.7428	458.6
	318	0.9999	12502.33	4.4323	-37.6016		453.9

Typically, ΔG_{ads}^0 values[5] around or equal to -20 kJ/mol indicate physisorption, while values equal to or more than -40 kJ/mol indicate chemisorption. The value of ΔG_{ads}^0 from this experiment indicates reversible physisorption adsorption on an energetically homogeneous adsorbent surface. The decrease in ΔG_{ads}^0 values at 318 K and the negative

sign for it indicate that the reaction ensured the adsorption process's spontaneity and the adsorbed layer's stability on the carbon steel surface. Adsorption for enthalpy ΔH_{ads}^0 could be calculated utilizing Vant' Hoff [25] Equation 5.

$$\text{Log } K_{\text{ads}} = -\frac{-\Delta H_{\text{ads}}}{2.303RT} + \text{Const} \quad (5)$$

when $\text{Log } K_{\text{ads}}$ is plotted against $1/T$, a linear line negative slope equal to $-\Delta H_{\text{ads}} / (2.303 \cdot R)$ is obtained, as illustrated in Figures 9 and 10. The thermodynamic method can estimate the entropy ΔS_{ads}^0 of inhibitors **A** and **S** using Equation 6.

$$\Delta G_{\text{ads}}^0 = \Delta H_{\text{ads}}^0 - T\Delta S_{\text{ads}}^0 \quad (6)$$

Based on the literature, if ΔH_{ads}^0 are negative, a thermal transmission to the environment occurs during adsorption, indicating an exothermic reaction. Conversely, if ΔH_{ads}^0 are positive, the heat transfer occurs from the medium to the system, indicating the reaction is endothermic[26].

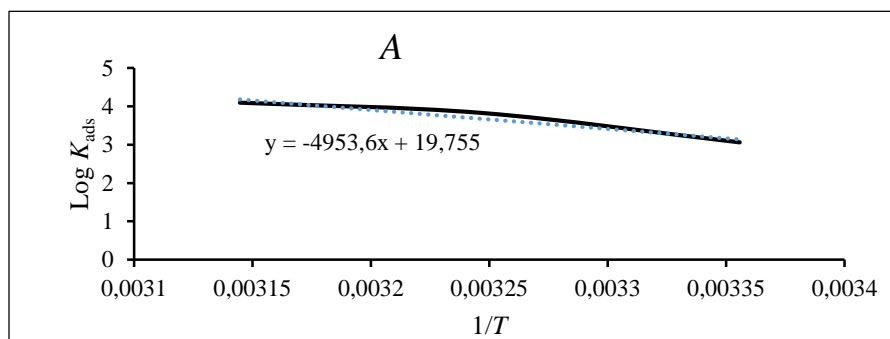


Figure 9. Correlation between $\text{Log } K_{\text{ads}}$ and $1/T$ for carbon steel N80 in a 1 M HCl solution with varying inhibitor concentrations of (**A**).

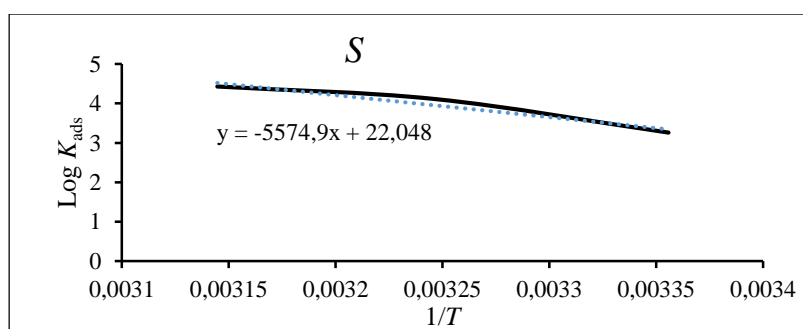


Figure 10. Correlation between $\text{Log } K_{\text{ads}}$ and $1/T$ for carbon steel N80 in a 1 M HCl solution with varying inhibitor concentrations of (**S**).

The study's findings imply that the inhibitor's adsorption is characterized by a positive ΔS_{ads}^0 data (94.8465, 106.7428) kJ/mol for inhibitors **A** and **S**, respectively, indicating chemisorption. So, the ΔS_{ads}^0 value is big and positive, indicating this is increased in disorder

upon transformation from a reactant towards the species adsorbed, which enhances adsorption on the metal surface.

4.2.4. Activation Energy (E_A)

Using the Arrhenius Equation 7 [27, 28], the activation energy of both inhibitors was investigated in an acidic medium at one molar concentration at various inhibitor concentrations and temperatures.

$$\text{Log } i_{\text{corr}} = \text{Log } A - \frac{E_a}{2.303RT} \quad (7)$$

where i_{corr} , A , E_a , R and T represent the corrosion current density, preexponential factor (the number of collisions in the inhibitor molecules), activation energy, universal gas constant $R=8.314 \text{ (J}\cdot\text{K}^{-1}\cdot\text{mol}^{-1})$ and temperature (K), respectively. By plotting $\text{Log } i_{\text{corr}}$ vs $1/T$, as in Figures 11 and 12, we get a straight line. From it, we deduce the value of the slope, which is

$\left(-\frac{E_a}{2.303RT}\right)$ and its intercept is $\text{Log } A$.

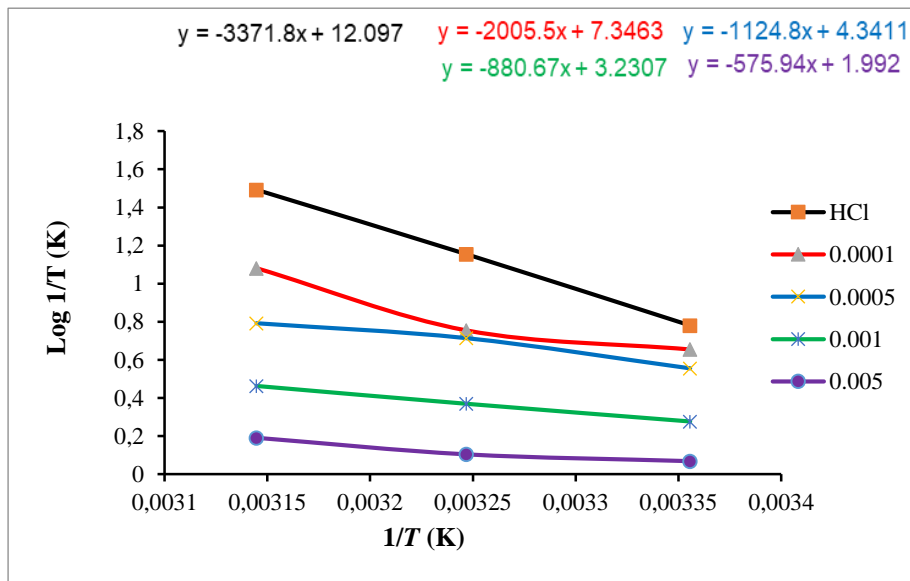


Figure 11. Arrhenius relationship in the absence and presence of inhibitor (A) for carbon steel N80 at temperatures of 298, 308 and 318 K.

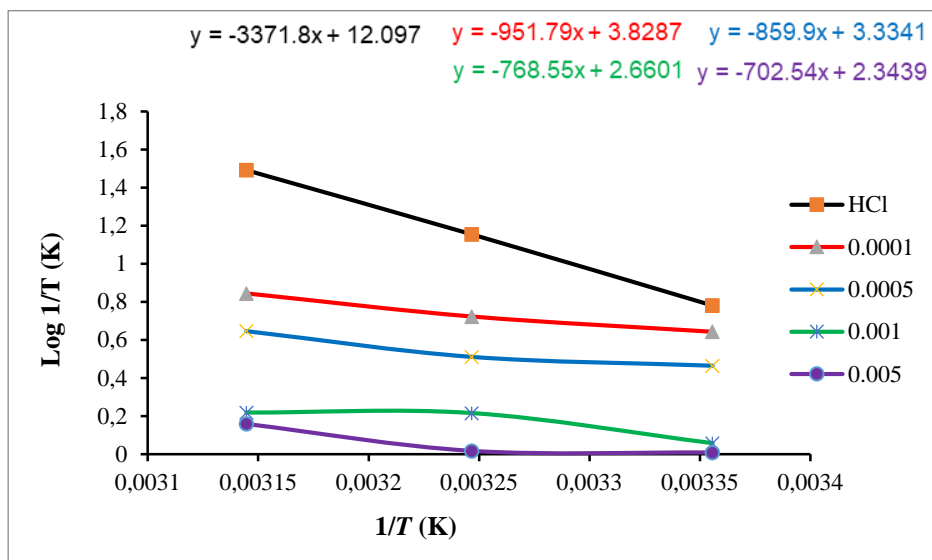


Figure 12. Arrhenius relationship in the absence and presence of inhibitor (S) for carbon steel N80 at temperatures of 298, 308 and 318 K.

From Table 3, because of the inhibitor molecules' gradual adsorption on carbon steel N80, we observe that the energy of activation (E_a) reduced with an increase in inhibitor concentration. As a result, during the experiment at higher temperatures, the experiment approached equilibrium more closely [29]. We also note that the number of collisions of the inhibitor molecules decreases with increasing concentration, indicating that chemical adsorption of the inhibitor molecules occurs on the surface of the carbon steel N80 alloy.

Table 3. The activation energy (E_a) and Arrhenius constant (A) values both in the absence and with inhibitors.

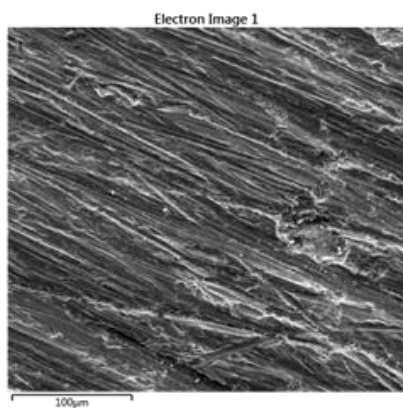
Compound	Conc. [M]	E_a [kJ/mol]	A
HCl blank	1	64.55	1.2507E+12
A	0.0001	38.39	2.219E+7
	0.0005	21.53	21935
	0.001	16.86	1701
	0.005	11.02	98.17
	S	0.0001	18.22
0.0005		16.46	2158
0.001		14.71	457.2
0.005		13.45	220.7

5. Scanning Electron Microscopy (SEM) and Energy-Dispersive X-ray Spectroscopy (EDS) analysis [30, 31]

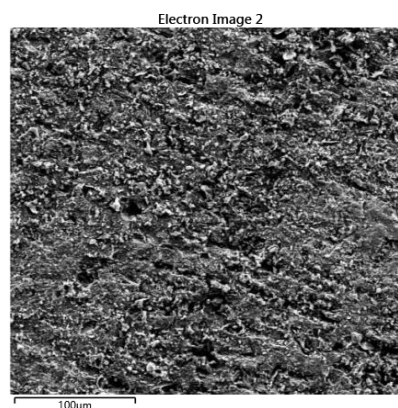
After both inhibitors **A** and **S** were immersed in a 1 M HCl solution for approximately 180 minutes, the metal surface morphology was examined by SEM spectroscopy. The polished mild steel surface seems smooth, as seen in Figure 13(a). On the other hand, as Figure 13(b) shows, the corrosive effects of 1 M HCl have left the mild steel's surface with defects and a rough texture. Figures 13(c) and (d) for **A** and **S** inhibitors, respectively, demonstrated the two specimens' perfect surface, free of visible holes or corrosion. Implies that the inhibitors **A** and **S** form a shield to stop corrosion on the carbon steel surface. The goal of the study was to identify the constituents of chemicals generated by the metal's outermost layer using 1 M HCl both with and without **A** and **S**. Directly, Figures 14(a, b), as well as (c), displays the EDS chart analysis on the identified places to SEM images for Figure 13(b, c), as well as (d). Through this measurement, we observe the weight and atomic percentages of the elements that make up the carbon steel N80 alloy after immersion in dilution concentration of hydrochloric acid and inhibitor solutions, as in Table 4. It was found that the percentage of oxygen is high in the acidic environment, but it is low in the inhibitor solution, as well as for the rest of the elements.

Table 4. EDX spectrum measurement shows the weight and atomic percentages of the elements composing the carbon steel alloy after immersion in hydrochloric acid and inhibitor solutions.

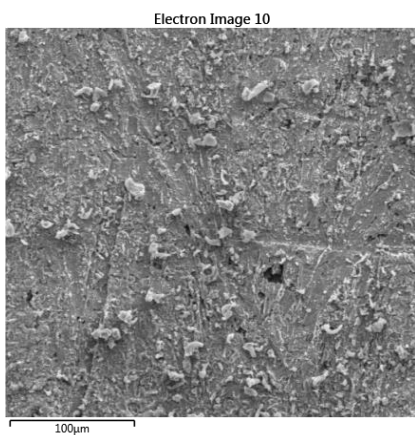
Elements		O	Cl	C	Fe
Sym.					
HCl (1 M)		10.70	3.02	4.24	70.22
A inhibitor	weight %	6.71	1.97	4.19	76.51
S inhibitor		5.52	1.22	5.13	76.73
HCl (1 M)		27.48	3.49	14.48	51.54
A inhibitor	atomic %	17.59	2.09	16.22	60.21
S inhibitor		15.18	1.52	18.80	60.48



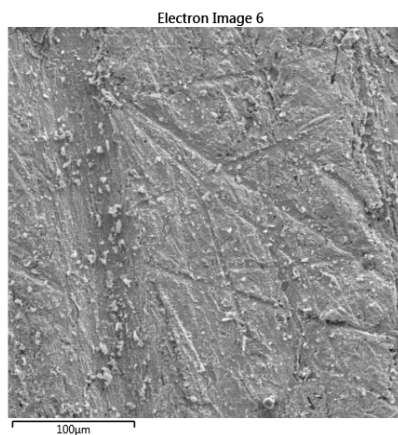
(a)



(b)

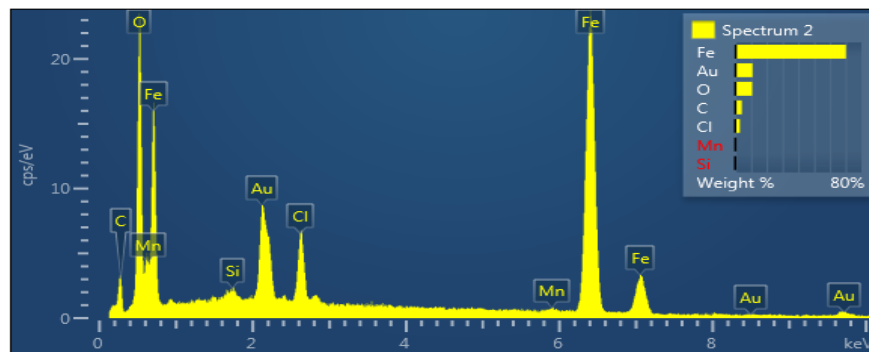


(c)

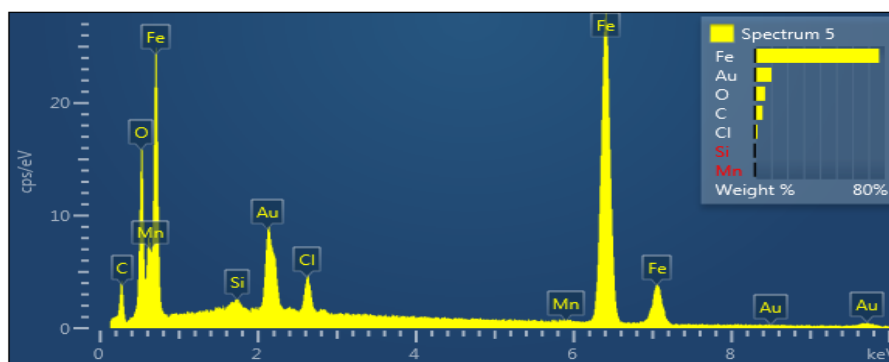


(d)

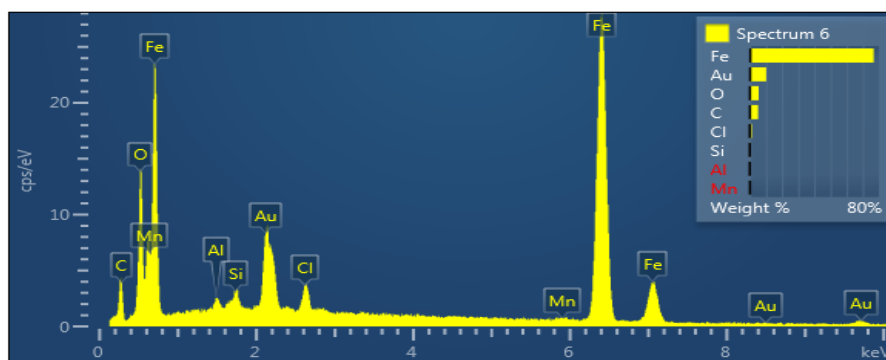
Figure 13. Photos for SEM of the mild steel N80 (a) specimen surface were polished before the immersion (b) after exposure to a 1 M HCl solution and (c, d) 1 M HCl solution containing 0.005 M of compound A and S.



(a)



(b)



(c)

Figure 14. EDX spectrum of mild steel N80 following contact with various solutions, (a) depicts the spectrum of the specimen surface subjected to a solution of 1 M HCl. Moreover, (b, c) displays the spectrum of the specimen surface subjected to a solution of 1 M HCl, which contains 0.005 M of A and S inhibitors.

Conclusion

The study's findings in this research showed that both the prepared compounds **A** and **S** are organic corrosion inhibitors, due to their adsorption on the surface of carbon steel N80 alloy, which confirmed this is the result of electrochemical polarization (Tafel curves) at different temperatures. By measuring the i_{corr} , E_{corr} and $IE\%$. We also noticed that compound **S** is more effective and inhibitory than compound **A** through the values of the results we obtained in this research ΔG^0 , ΔS^0 , ΔH^0 , C_R , θ and E_A for the reason that the azomethine group is more effective than the azo group and the presence of aromatic rings and substituted groups, the type of adsorption is chemical. SEM and EDS techniques were also studied to confirm these results.

Acknowledgment

We appreciate the cooperation of the deanship of the college of education for pure sciences at the University of Basra. We also appreciate the assistance of the head of the chemistry department at the college of education for pure sciences at the University of Basra for facilitating many of the obstacles that accompanied this work.

Authors' Declaration

- Conflicts of interest: None.
- We hereby confirm that all the Figures and Tables in the manuscript are ours. Besides, have been given permission for republication attached to the manuscript.
- Ethical clearance: the project was approved by the local ethical committee at the University of Basrah.

Authors' Contribution Statement

Abeer Mohammed Jabbar participated in the following roles: conducting and following up all reactions, measuring spectra of the prepared compounds, and following the corrosion measurements of the prepared compound **A** and **S**.

Adnan Sultan Abdalnabi participated in the following roles: the help interpretation of the spectra data of the prepared compounds, corrosion measurements of the prepared compound, and the interpretation of their results, manuscript review and proofreading.

References

1. M.S.B. Reddy, D. Ponnamma, K.K. Sadasivuni, S. Aich, S. Kailasa, H. Parangusan, M. Ibrahim, S. Eldeib, O. Shehata, M. Ismail and R. Zarandah, Sensors in advancing the capabilities of corrosion detection: A review, *Sens. Actuators A*, 2021, **332**, 113086. doi: [10.1016/j.sna.2021.113086](https://doi.org/10.1016/j.sna.2021.113086)

2. S. Zehra, M. Mobin and J. Aslam, An overview of the corrosion chemistry, *Environmentally Sustainable Corrosion Inhibitors*, 2022, pp. 3–23. doi: [10.1016/B978-0-323-85405-4.00012-4](https://doi.org/10.1016/B978-0-323-85405-4.00012-4)
3. G. Jiang, D. Xu, P. Feng, S. Guo, J. Yang and Y. Li, Corrosion of FeCrAl alloys used as fuel cladding in nuclear reactors, *J. Alloys Compd.*, 2021, **869**, 159235. doi: [10.1016/j.jallcom.2021.159235](https://doi.org/10.1016/j.jallcom.2021.159235)
4. A.A. Al-Amiery, W.N. Roslam, W. Isahak and W. K. Al-Azzawi, Corrosion inhibitors: natural and synthetic organic inhibitors, *Lubricants*, 2023, **11**, 174. doi: [10.3390/lubricants11040174](https://doi.org/10.3390/lubricants11040174)
5. A. Kadhim, N. Betti, H.A. Al-Bahrani, M.K.S. Al-Ghezi, T. Gaaz, A.H. Kadhum and A. Alamiery, A mini review on corrosion, inhibitors and mechanism types of mild steel inhibition in an acidic environment, *Int. J. Corros. Scale Inhib.*, 2021, **10**, no. 3, 861–884. doi: [10.17675/2305-6894-2021-10-3-2](https://doi.org/10.17675/2305-6894-2021-10-3-2)
6. B.C. Sahu, *Organic Corrosion Inhibitors*, IntechOpen, 2023. doi: [10.5772/intechopen.109523](https://doi.org/10.5772/intechopen.109523)
7. L. Chen, D. Lu and Y. Zhang, Organic compounds as corrosion inhibitors for carbon steel in HCl solution: A Comprehensive Review, *Materials*, 2022, **15**, no. 6, 2023. doi: [10.3390/ma15062023](https://doi.org/10.3390/ma15062023)
8. D.K. Verma, C. Verma and J. Aslam, Computational modelling and simulations for designing of corrosion inhibitors, *Elsevier*, 2023, 525–548. doi: [10.1016/C2021-0-02414-7](https://doi.org/10.1016/C2021-0-02414-7)
9. D. Mamand and H. Qadr, Quantum computations and density functional theory on corrosion inhibition efficiency of BIA, HBT, MBI and PIZ compounds, *Хімія, фізика та технологія поверхні*, 2023, **14**, no. 2, 159–172. doi: [10.15407/hftp14.02.159](https://doi.org/10.15407/hftp14.02.159)
10. J. Chen, X. Xie, J. Liu, Z. Yu and W. Su, Revisiting aromatic diazotization and aryl diazonium salts in continuous flow: highlighted research during 2001–2021, *React. Chem. Eng.*, 2022, **7**, no. 6, 1247–1275. doi: [10.1039/D2RE00001F](https://doi.org/10.1039/D2RE00001F)
11. F. Almashal, A.M. Jabar and A.M. Dhumad, Synthesis, characterization and DFT computational studies of new heterocyclic azo compounds, *Eur. J. Chem.*, 2018, **9**, no. 2. doi: [10.5155/eurjchem.9.2.84-88.1683](https://doi.org/10.5155/eurjchem.9.2.84-88.1683)
12. S.H. Sumrra, I. Sahrish, M.A. Raza, Z. Ahmad, M.N. Zafar, Z.H. Chohan, M. Khalid and S. Ahmed, Efficient synthesis, characterization, and in vitro bactericidal studies of unsymmetrically substituted triazole-derived Schiff base ligand and its transition metal complexes, *Monatsh. Chem.*, 2020, **151**, no. 4, 549–557. doi: [10.5772/intechopen.109523](https://doi.org/10.5772/intechopen.109523)
13. N.Q. Trung, P.T.P. Nam and N.V. Tuyen, Synthesis, characterization and anticancer properties of platinum(II) complexes bearing chiral azomethine ligands, *Vietnam J. Chem.*, 2021, **59**, no. 2, 221–228. doi: [10.1002/vjch.202000159](https://doi.org/10.1002/vjch.202000159)

14. Q.T. Nguyen, P.N.P. Thi, Q.D. Bui and V.T. Nguyen, Spectral characterization and biological activities of some metal complexes bearing an unsymmetrical salen-type ligand, (Z)-1-(((2-((E)-(2-hydroxy-6-methoxybenzylidene)amino)phenyl)amino)methylene) naphthalen-2(1H)-one, *Heteroat. Chem.*, 2023, **8**, 2023. doi: [10.1155/2023/4563958](https://doi.org/10.1155/2023/4563958)
15. J. Geethapriya, A.R. Devaraj, K. Gayathri, R. Swadhi, N. Elangovan, S. Manivel, S. Sowrirajan and R. Thomas, Solid state synthesis of a fluorescent Schiff base (E)-1-(perfluorophenyl)-N-(o-toly)methanimine followed by computational, quantum mechanical and molecular docking studies, *Results Chem.*, 2023, **5**, 100819. doi: [10.1016/j.rechem.2023.100819](https://doi.org/10.1016/j.rechem.2023.100819)
16. Q.T. Nguyen, Q.H. Lam, P.N.P. Thi and V.T. Nguyen, Synthesis, characterization and in vitro cytotoxicity of platinum (II) complexes with some tetradentate salen ligands, *Sci. J. Chem.*, 2019, **7**, no. 2, 49–55. doi: [10.11648/j.sjc.20190702.13](https://doi.org/10.11648/j.sjc.20190702.13)
17. F. Ge, X. Huang, Y. Zhang, Y. Song, X. Meng, H. Ge and Y. Zhao, Corrosion behavior of 2205 DSS base metal and ER 2209 weld metal in a deposited ash/water suspension, *Int. J. Electrochem. Sci.*, 2021, **16**, no. 7, 210717. doi: [10.20964/2021.07.35](https://doi.org/10.20964/2021.07.35)
18. A. Sehmi, H.B. Ouici, A. Guendouzi, M. Ferhat, O. Benali and F. Boudjellal, Corrosion inhibition of mild steel by newly synthesized pyrazole carboxamide derivatives in HCl acid medium: experimental and theoretical studies, *J. Electrochem. Soc.*, 2020, **167**, no. 15, 155508. doi: [10.1149/%201945-7111/abab25](https://doi.org/10.1149/%201945-7111/abab25)
19. K. Raviprabha and R.S. Bhat, Corrosion inhibition of mild steel in 0.5 M HCL by substituted 1,3,4-oxadiazole, *Egypt. J. Pet.*, 2023, **32**, no. 2, 1–10. doi: [10.1016/j.ejpe.2023.03.002](https://doi.org/10.1016/j.ejpe.2023.03.002)
20. M. Ikpi, F.E. Abeng and B. Okonkwo, Experimental and computational study of levofloxacin as corrosion inhibitor for carbon steel in acidic media, *World News Nat. Sci.*, 2017, **9**, 79–90. doi: [publication/318442519](https://doi.org/publication/318442519)
21. Y. Elkhofia, I. Forsala, E.M. Rakiba and B. Mernari, The inhibition action of essential oil of *Juniperus Phoenicia* on the corrosion of mild steel in acidic media, *Port. Electrochim. Acta.*, 2018, **36**, no. 2, 77–87. doi: [10.4152/pea.201802077](https://doi.org/10.4152/pea.201802077)
22. G. Palumbo, M. Gorny and J. Banas, Corrosion inhibition of pipeline carbon steel (N80) in CO²⁻ saturated chloride (0.5 M of KCl) solution using gum arabic as a possible environmentally friendly corrosion inhibitor for shale gas industry, *J. Mater. Eng. Perform.*, 2019, **28**, no. 10, 6458. doi: [10.1007/s11665-019-043793](https://doi.org/10.1007/s11665-019-043793)
23. A. Kokalj, On the use of the Langmuir and other adsorption isotherms in corrosion inhibition, *Corros. Sci.*, 2023, **217**, 111112. doi: [10.1016/j.corsci.2023.111112](https://doi.org/10.1016/j.corsci.2023.111112)
24. S.A. Umoren, M.J. Banera, T. Alonso-Garcia, C.A. Gervasi and M.V. Mirifico, Inhibition of mild steel corrosion in HCl solution using chitosan, *Cellulose*, 2013, **20**, no. 5, 2529–2545. doi: [10.1007/s10570-013-0021-5](https://doi.org/10.1007/s10570-013-0021-5)

-
25. S.K. Ahmed, W.B. Ali and A.A. Khadom, Synthesis and investigations of heterocyclic compounds as corrosion inhibitors for mild steel in hydrochloric acid, *Int. J. Ind. Chem.*, 2019, **10**, no. 2, 159–173. doi: [10.1007/s40090-019-0181-8](https://doi.org/10.1007/s40090-019-0181-8)
 26. D. Daoud, T. Douadi, S. Issaadi and S. Chafaa, Adsorption and corrosion inhibition of new synthesized thiophene Schiff base on mild steel X52 in HCl and H₂SO₄ solutions. *Corros. Sci.*, 2014, **79**, 50–58. doi: [10.1016/j.corsci.2013.10.025](https://doi.org/10.1016/j.corsci.2013.10.025)
 27. A.F.S.A. Rahiman and S. Sethumanickam, Corrosion inhibition, adsorption and thermodynamic properties of poly(vinyl alcohol-cysteine) in molar HCl, *Arabian J. Chem.*, 2017, **10**, S3358–S3366. doi: [10.1016/j.arabjc.2014.01.016](https://doi.org/10.1016/j.arabjc.2014.01.016)
 28. L.C. Go, D. Depan, W.E. Holmes, A. Gallo, K. Knierim, T. Bertrand and R. Hernandez, Kinetic and thermodynamic analyses of the corrosion inhibition of synthetic extracellular polymeric substances, *PeerJ Mater. Sci.*, 2020, **2**, e4. doi: [10.7717/peerj-matsci.4](https://doi.org/10.7717/peerj-matsci.4)
 29. P.P. Kumari, P. Shetty and S.A. Rao, Electrochemical measurements for the corrosion inhibition of mild steel in 1 M hydrochloric acid by using an aromatic hydrazide derivative, *Arabian J. Chem.*, 2017, **10**, no. 5, 653–663. doi: [10.1016/j.arabjc.2014.09.005](https://doi.org/10.1016/j.arabjc.2014.09.005)
 30. Z. Belarbi, S. Nestic and F. Farelas, Effect of operating parameters on the inhibition efficacy of decanethiol, *NACE Int. Corros. Conf. Expo*, 2018, 10823. doi: [publication/324706143](https://doi.org/publication/324706143)
 31. Y.U. Ting, F. Zhang, L. Zhao, L.U. Xianjin and S. Xie, Crack failure analysis of stainless steel seamless pipe, *Zhejiang Academy of Special Equipment Science*, 2023, **4**, 98–103. doi: [10.3233/ATDE230446](https://doi.org/10.3233/ATDE230446)

